Research Article

28

INDONESIAN SCHOLAR SOCIETY

Indones. J. Chem. Stud.
2025, 4(1), 28–34
Available online at journal.solusiriset.com
e-ISSN: 2830-7658; p-ISSN: 2830-778X

Indonesian Journal of Chemical Studies

Fabrication and Characterization of Graphene Nanoplatelets/Zinc Oxide Nanocomposites as a Military Radar Absorbing Material

Anselmo Bima Rasendriya[1]*, Andri Hardiansyah[2], Gita Resty Amalia[1], Ismail Rahmadtulloh[3,4], Andi Setiono[5], M. Zuhnir Piliang[1], Hotma Renta[1]

[1]*Department of Physics, The Republic of Indonesia Defense University, Bogor 16810, Indonesia*

[2]*Research Center for Nanotechnology Systems, National Research and Innovation Agency (BRIN), Banten 15314, Indonesia*

[3]*Department of Mechanical Engineering, National Taiwan University of Science and Technology, Taipei City 106335, Taiwan*

[4]*Department of Materials Engineering, Ming Chi University of Technology, New Taipei City 24301, Taiwan*

[5]*Research Center for Photonics, National Research and Innovation Agency (BRIN). Banten 15314, Indonesia*

Received: 24 Mar 2025; Revised: 20 Apr 2025; Accepted: 23 Apr 2025;
Published online: 16 Jun 2025; Published regularly: 30 Jun 2025

Abstract— Stealth aircraft have the capability to intercept radar waves. One common technique involves the use of radar-absorbing materials (RAMs). This study focused on the synthesis of advanced lightweight functional materials derived from advanced carbon and semiconductor compounds for microwave absorbing through mechanical homogenization. Graphene nanoplatelets (GNP) and Zinc Oxide (ZnO) possess excellent dielectric and magnetic loss capability due to their thermal conductivity, small particle size, large surface area, disordered structure, and lightweight nature. The GNP and ZnO were developed as advanced carbon and semiconductor nanocomposites using Planetary Ball Milling (PBM) at a ratio of 1:1. This approach aimed to improve the structure, morphology, and electromagnetic performance of the materials. A comparison between the nanocomposite materials and their precursors was conducted to clarify the advantages of using nanocomposites. FE-SEM showed the layered carbon sheets in GNP. XRD exhibited the alteration in the crystallite structure of ZnO, while FTIR spectroscopy confirmed the presence of specific functional groups. In addition, the GNP/ZnO nanocomposites showed strong microwave polarization capabilities. Notably, the GNP/ZnO nanocomposite achieved the lowest RL value compared to the precursor materials with a value of -28.21 dB at 8.45 GHz and a thickness of 3 mm in the scope of X-band range. While the through power was calculated at 99.84%. Through mechanical homogenization, a well-structured disordered crystallite layered material was fabricated for military RAMs. In the industrial sector, GNP/ZnO nanocomposites showed promising potential as a lightweight and advanced functional material for future stealth aircraft applications.

Keywords— *Graphene nanoplatelets; Nanocomposites; Planetary ball milling; Radar absorbing material; Zinc dioxide*

1. INTRODUCTION

In the military realm, Radar Absorbing Materials (RAMs) are essential in stealth aircraft as an innovation to deceive radar systems. A radar is an electromagnetic device capable of mapping an area around the device by emitting electromagnetic (EM) signals and receiving echoes to create a detailed image of the surroundings [1]. By absorbing and redirecting the EM signals emitted by radar through polarization, stealth aircraft can work effectively [2]. RAMs function by leveraging the polarization of EM waves that occur on the disordered surface of the material and transforming them into thermal energy [3].

Microwave absorbing materials (MAMs) were related to their complex permittivity and permeability [4] . These properties lead to dielectric and magnetic loss of the material. The ability to absorb EM waves represents with reflection loss (RL) value. The complex permittivity and permeability were connected to RL

***Corresponding author**.
Email address: anselmorasendriya@gmail.com
DOI: 10.55749/ijcs.v4i1.69

value through the transmission line theory in Eq. (3) and (4) [4, 5]. According to Eq. (3) and (4), RL value depends on impedance matching, dielectric loss and magnetic loss through interface and dipole polarization [6]. Therefore, the material will exhibit strong microwave attenuation, and excellent impedance matching [5].

The microwave-absorbing properties of the nanocomposites are observed using a Vector Network Analyzer (VNA). The S_{11} parameter is used to obtain the RL and the through power values. RL quantifies electromagnetic (EM) wave absorption capability derived from relative complex permittivity and permeability [7]. The lowest RL indicates a higher possibility of polarization.

The potential and unique properties of carbon make the development of carbon-based MAMs a current trend. Carbon is characterized by their low density, adjustable conductivity, large surface area, anticorrosion properties, lightweight nature, and a strong ability to absorb electromagnetic waves [8, 9]. The specific properties of carbon materials can be adjusted, such as dielectric loss and surface chemistry, by attaching functional groups to their surface [3]. A carbon currently being developed is graphene nanoplatelets (GNPs). GNPs describe advanced multilayer graphene in a graphite nanostructure [10, 11].

GNPs exhibit excellent mechanical properties, such as strength between ~100-400 GPa, resistivity of 50 μΩ cm (in-plane), thermal conductivity, expansion, stability in 5,300 $Wm^{-1}K^{-1}$ (in-plane), -1 x $10^{-6}K^{-1}$ (in-plane), and 450-650 ℃ (in air), with specific surface area of 100-1000 m^2/g up to 2600 m^2/g [11, 12]. Therefore, one way to utilize the outstanding properties of these nanostructures is to use them as reinforcing elements in composite structures. Therefore, GNPs are well-suited as thermal interface materials and reinforce components in composite structures [13].

Moreover, ZnO is a semiconductor with excellent attenuation and impedance matching [14]. The oxygen functional groups in ZnO cause defects in the structure that lead to interfacial and dipole polarization, which improve the microwave absorbing properties due to its excellent dielectric loss [15]. Therefore, ZnO is suitable for military RAM, combined with its lightweight and flexible properties [16]. However, to enhance the microwave absorption properties, carbon is combined with semiconductors through PBM to develop a nanocomposite.

The primary objective of utilizing PBM is to modify the particles, in particular, to reduce the particle size of the materials [17]. This condition increases surface area and promotes polarization. The use of the PBM method is proposed for safer, simpler, low-cost, and environmentally friendly experiments through green synthesis technology [18]. This method does not require a solution between the experiment, either non or hazardous solvents.

However, studies about GNP/ZnO nanocomposites using PBM have not been widely investigated. Recent studies have shown that carbon and semiconductor-based composites have outstanding microwave absorption performance. Chen, et al. have synthesized ZnO/porous carbon using solvent-free conditions and pyrolyzed at three conditions, which obtain an RL value of -41.7 dB at 14.5 GHz [19]. Several works have also shown that MWCNT/ZnO and GNPs/ZnO obtain RL values of -26.4 dB at 11.2 GHz and -44.8 dB at 4.65 GHz respectively, using high-energy milling and facile reaction methods [20, 21].

Recent studies show that the performance of microwave absorption is influenced by several factors, including dielectric loss, magnetic loss, and impedance matching within the material. These factors are affected by interface and dipole polarization caused by porous, disordered, or amorphous structures. This particular research focuses on a composite structure composed of carbon and ZnO. The following issues was related to this study.

In this study, nanocomposites are successfully synthesized from GNP as carbon sources and ZnO as semiconductors using PBM through green synthesize. We characterized the structure and morphology of the materials using field-emission scanning electron microscopy with electron-dispersive X-ray (FE-SEM EDX) and X-ray diffraction (XRD). We evaluate the microwave absorption by using VNA to determine the reflection loss at the frequency range of 8-12 GHz (X-band).

2. EXPERIMENTAL SECTION

2.1. Materials

This research used GNPs and ZnO as precursor materials. Commercial GNPs grade C-750 was purchased from Sigma Aldrich, USA. The ZnO grade AR with 99% purity was obtained from Loba Chemie. Commercial ZnO was classified as a wurtzite crystallite type, which referred to XRD analysis.

2.2. Instrumentation

Nanocomposites were mechanically synthesized with PBM PM 400 (Retsch, Germany). The structure and morphology of the materials were characterized by FE-SEM EDX (JEOL JSM-IT700HR, Japan), and XRD (PANalytical, X'pert, Netherlands). The functional groups of all materials were confirmed by FTIR spectroscopy (Thermoscientific Nicolet iS-10). VNA Master Anritsu MS2038C (Japan) was used to test the performance of the materials. Data analysis was evaluated by ORIGIN 2021 Software.

2.3. Synthesis of GNPs/ZnO

Commercial GNPs and ZnO were used as precursor materials. First, GNPs and ZnO were prepared with a

ratio of 1:1. GNPs and ZnO were then homogenized with PBM. The homogenization process was carried out with four stainless steel balls for 3 h at 300 rpm. Next, the sample was sieved using 400-mesh sieve to remove impurities.

2.4. Structure and Morphology Characterization

The sample micrographs were taken under 10 kV accelerating voltage in the secondary electron mode with 4 K times magnification, which corresponded to a 10 µm size scale bar on the images. The crystallite structure of the materials was analyzed using XRD with a 40 kV voltage and 30 mA current. The measurement was taken at an incidence angle of 1° with Cu radiation in the 2θ 20-90°. The functional groups of each material were analyzed in the range of 400-4000 cm^{-1} under infrared radiation.

2.5. Microwave Absorption Performance

The GNP/ZnO nanocomposites were analyzed using VNA based on 3 mm thickness and X-band frequency. A two-port network was used to test the performance of the nanocomposites. The response of the port network was described by S_{11}, S_{12}, S_{21}, and S_{22} [22]. The RL values were confirmed by VNA at S_{11} port using the Nicolas-Ross-Weir algorithm [23].

3. RESULT AND DISCUSSION

3.1. Formation Mechanism of Fabricating GNP/ZnO Nanocomposites

The formation mechanism of the GNP/ZnO nanocomposite is illustrated in **Fig. 1**. GNPs and ZnO were prepared in a PBM vial at a ratio of 1:1. The GNP and ZnO were then mechanically homogenized. As shown in **Fig. 1**, the process successfully resulted in the synthesis of the GNP/ZnO nanocomposite.

The particle sizes of each material were decreased by PBM, as detailed in **Table 1.** The GNP/ZnO nanocomposite consists of a mechanical interlocking bond. This condition directly affects the structure and morphology of the GNP/ZnO nanocomposite compared to the precursor materials. Mechanical interlocking describes strong interfacial bonding [24]. GNPs and ZnO are easily interracially bonded due to their disordered and defective structure.

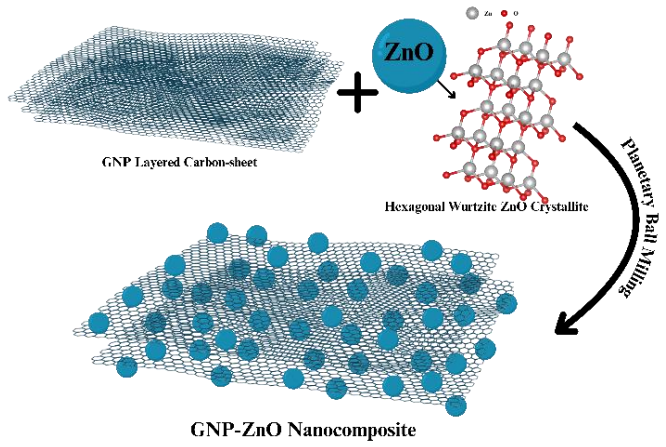

Fig. 1. Schematic formation mechanism of GNPs/ZnO Nanocmposites

Table 1. Value of crystallite size and crystallinity percentage of materials

Material	Size (nm)	Percentage (%)
ZnO	63.4	82.95
GNP/ZnO	19.3	81.8

3.2. Characterization of Structure and Morphology

The FE-SEM image results of GNP are shown in **Fig. 2(a).** GNP was observed as layered carbon sheets. The layered surface was composed of a disordered layer, which developed into a stacking layer. This structure may cause a polarization interface to occur [25]. Therefore, the GNP can be characterized as an amorphous material. Additionally, **Fig. 2(b-d)** show the EDS mapping of GNP, in which the carbon and oxygen elements were evenly distributed. Furthermore, based on the data in **Fig. 3(a)**, carbon was the highest content of GNP. It refers to the high purity of the GNP.

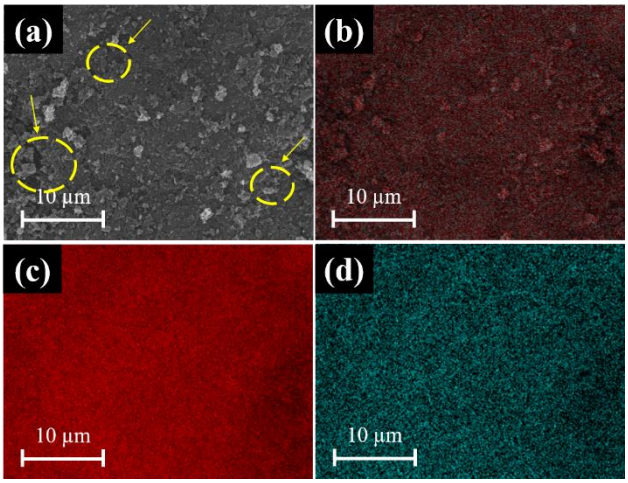

Fig. 2. FE-SEM Images of (a) GNP: The marks show the layered-carbon sheets and its EDS mapping for (b) combined element image, (c) C, and (d) O Elements

The microstructure and morphology of GNP/ZnO nanocomposites are illustrated in **Fig. 4(a)**, while **Fig. 4(b-e)** provides EDS mapping of the elements. The data showed the GNP/ZnO nanocomposites formed a crystallite structure with layered sheets. This crystallite layered sheet structure is arranged by disordered layers. The FE-SEM images of GNP/ZnO nanocomposites indicated that the GNP was well combined with the ZnO. Based on **Fig. 3(b)**, the GNP/ZnO nanocomposites contained a high carbon content, specifically 79.7%, along with 11.9% oxygen, and 8.45% zinc. The GNP/ZnO nanocomposites were observed as a disordered crystallite layered-structure material, which

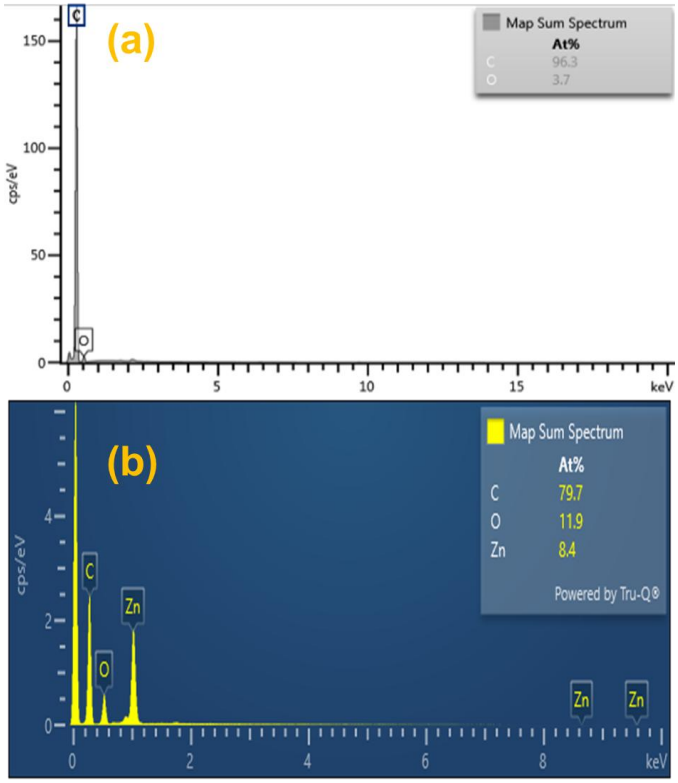

Fig. 3. FE-SEM EDS mapping spectrum of (a) GNP, and (b) GNP/ZnO Composite

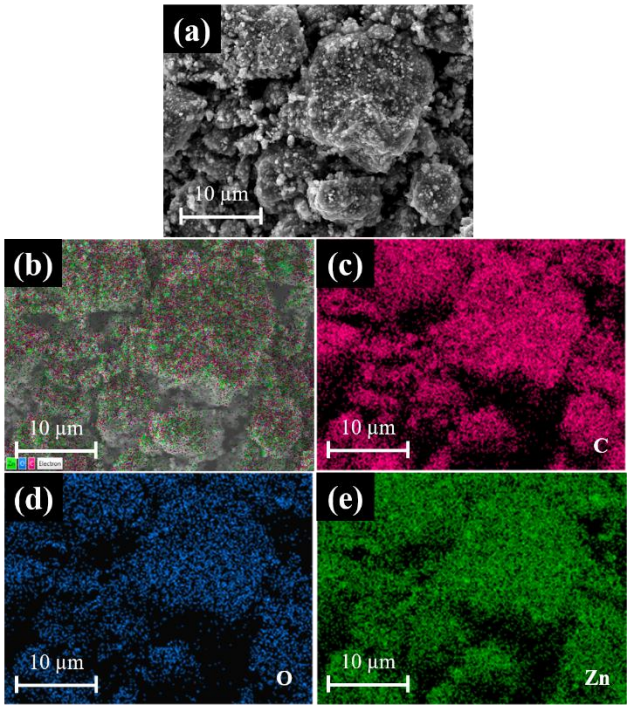

Fig. 4. FE-SEM Images of (a) GNP/ZnO Nanocomposites and its EDS mapping for (b) Combined Element Image, (c) C, (d) O, and (e) Zn Elements.

confirmed by the XRD results. This disordered crystallite-layered structure significantly affect the microwave absorbing performance of the materials. This structure triggers the polarization of the microwave, which in turn causes reflection loss (RL). This effect is clearly demonstrated in the observed microwave absorption performance.

The X-ray diffractograms of all materials were evaluated in the 2θ range of 20-90°. The X-ray diffractograms of GNP were confirmed by JCPDS 98-007-6767. As shown in **Fig. 5(a)**, GNP showed two primary peaks at 2θ values of 26° and 44°. The peak 2θ at 26° was evaluated as a (002) plane with a hexagonal crystal system [26]. The GNP crystallite planar system is based on the FE-SEM observations, which revealed that GNP consists of layered carbon sheets. The 2θ peak at 26° corresponds to a 3.36 nm interlayer space. Similarly, the 2θ peak at 44° was identified as the (011) plane, corresponding to an interlayer spacing of 2.03 nm. This value represents the space between crystals under the X-ray. The high intensity of these two primary peaks confirms the purity of the GNPs.

Fig. 5(b) shows several significant peaks of ZnO. These peaks were analyzed using XRD and confirmed with JCPDS 98-006-7574. The crystallites of ZnO were analyzed as a hexagonal crystal system and classified as a wurtzite crystal type. The analyzed peaks were confirmed with (010), (002), (002), (011), (012), (110), (013), (112), and (021) miller index, at the 2θ peaks of 31°, 34°, 36°, 47°, 56°, 62°, 66°, 67°, and 69°, respectively. The XRD pattern exhibited perfect peaks of ZnO, corresponding to non-impurities with an incredibly high-intensity value. These findings confirm the purity of ZnO.

The X-ray diffractograms of GNP/ZnO nanocomposites are presented in **Fig. 5(c)**. As illustrated in **Fig. 5(b-c)**, the GNP/ZnO nanocomposites perfectly exhibited distinct crystallite peaks of ZnO. Moreover, the carbon peak of GNP was evaluated at the 2θ peak of 26°. Although the peak intensity of GNP was relatively low, the presence of GNP was confirmed in the GNP/ZnO nanocomposites. The presence of GNP and ZnO peaks in **Fig 5(c)** indicates that the disordered crystallite-layered structure of GNP/ZnO nanocomposites was successfully fabricated. In addition, the intensity of GNP and ZnO decreased significantly compared to GNP/ZnO nanocomposites. This trend occurs due to changes in the crystalline phase between the precursor materials and GNP/ZnO nanocomposites [27]. Overall, these findings indicate that GNP/ZnO nanocomposites is successfully formed.

The particle size of the crystallite was calculated using the Scherrer [28]:

$$D = \frac{k\lambda}{\beta_{hkl} \cos \theta_{hkl}} \quad (1)$$

where, k is a constant related to crystallite shape (0.9), λ is the X-ray wavelength (0.154 nm), β_{hkl} is the FWHM number, and θ_{hkl} is the peak position.

The crystallite particle size value of ZnO and GNP/ZnO nanocomposites were calculated using the Scherrer **Eq. (1)**. The following crystallite size was referred to the FWHM number of the significant peaks of each material. Moreover, the crystallinity percentage

of ZnO and GNP/ZnO nanocomposites was also determined. The following measurement was conducted using the area of crystalline peaks (A_c) and the area of all peaks (A_p) in **Eq. (2)** [29, 30].

$$D = \frac{A_C}{A_P} \times 100\% \quad (2)$$

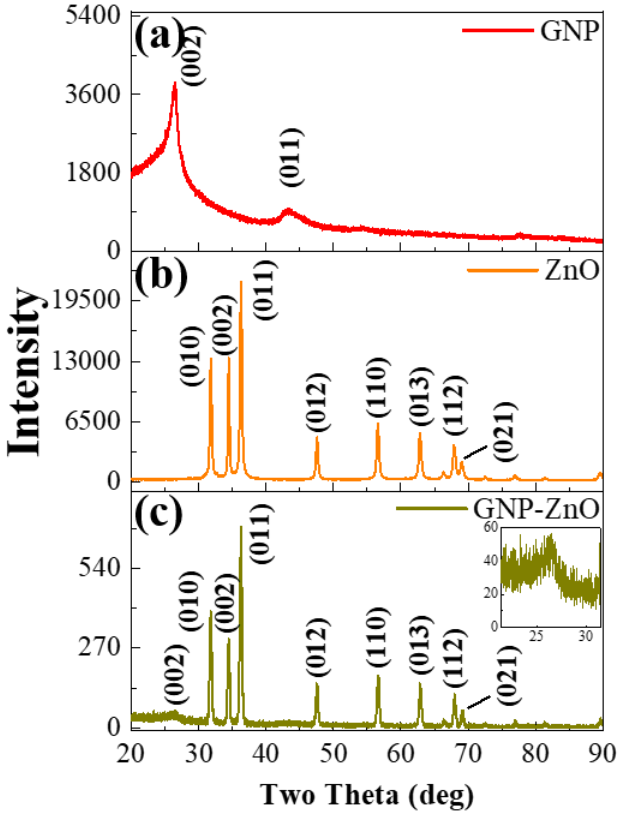

Fig. 5. X-Ray Diffractogram results of (a) GNP, (b) ZnO, and (c) GNP/ZnO Nanocomposites

Based on **Table 1**, the crystallite size and the crystalline percentage value of ZnO were decreased compared to GNP/ZnO nanocomposite. The decreasing of crystallite size and the crystalline percentage value indicates the presence of ZnO crystal impurities in the GNP/ZnO nanocomposites. However, this impurity indicates that the GNPs are successfully composed with ZnO, which refers to the disordered crystallite-layered structure of GNP/ZnO nanocomposites in FE-SEM images (**Fig. 4**).

The FTIR spectra was obtained through infrared reflection in the range of 400-4000 cm^{-1}. **Fig. 6** represents the functional groups of ZnO and carbon bonds. The fingerprint peaks of ZnO were identified at 436 and 420 cm^{-1} [31, 32]. The shifting is a result of the interaction between GNP and ZnO. In addition, the simultaneous peak exhibited around 3400 cm^{-1} by all materials represented the stretching vibration of O-H bonds [31–33]. Furthermore, the peaks observed in the range of 1638 – 1169 cm^{-1} were attributed to the presence of carbon bonds from environmental moisture [31–34]. These peaks indicate that the GNP/ZnO nanocomposites are successfully synthesized.

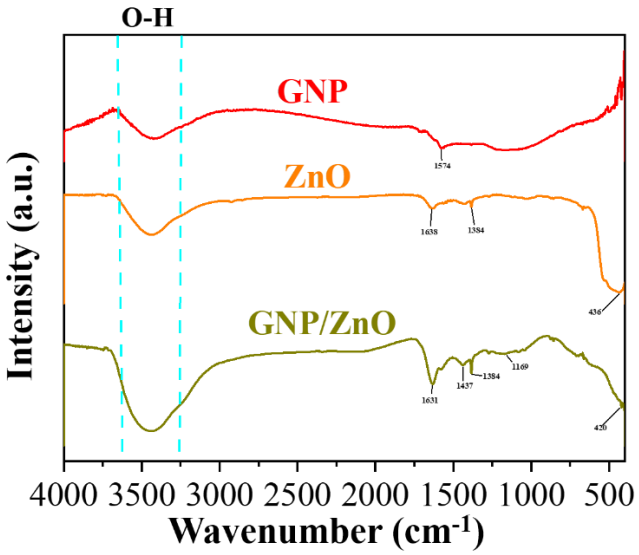

Fig. 6. FT-IR spectra of ZnO and GNP/ZnO

3.3. Microwaves Absorbing Performance

The microwave absorption performance was evaluated using VNA. The Nicolas-Ross-Weir algorithm is used to calculate the S_{11}, which RL value is obtained [5]. The Nicolas-Ross-Weir algorithm is shown by **Eq. (3)** and **(4)**.

$$Z_{in} = z_0\sqrt{\mu_r/\varepsilon_r}\tanh[j(2\pi fd)/c\sqrt{\mu_r/\varepsilon_r})] \quad (3)$$

$$RL = 20\log\left|\frac{(Z_{in}-Z_o)}{(Z_{in}+Z_o)}\right| \quad (4)$$

Where Z_{in} and Z_o repsent the input impedance of the absorber and the impedance of empty space respectively, while μ_r and ε_r are complex permeability and permittivity, *f* is frequency, *d* and *c* are thickness and light's velocity.

The through power of the materials was calculated using **Eq. (5)** and **(6)**, which used the RL value [35]:

$$|\tau| = 10^{\text{reflection loss}/20} \quad (4)$$

$$Through\ power\ (\%) = (1-\tau)\times 100\% \quad (5)$$

Based on **Fig. 7** and **Table 3**, all materials showed four significant RL peaks. The lowest peak of all materials was displayed by GNP/ZnO nanocomposites with a value of -28.21 dB at 8.45 GHz, while the through power was evaluated at 99.85%. In more detail, in the scope of ZnO, the lowest RL was shown at 8.58 GHz with -20.08 dB and 99.08% through power. For GNP, -27.01 dB at a frequency of 8.42 GHz was evaluated as the lowest RL with the a through power value of 99.8%. All evaluated materials showed a minimum RL value of 8.4 GHz.

These results were influenced by the structure and morphology of the material. The GNP/ZnO nanocomposites were observed as the most complex structure and morphology, with the observed functional groups. The disordered crystallite layered-structure of

GNP/ZnO nanocomposites allows the dielectric loss to occur, which leads to interface and dipole polarization [36]. Furthermore, the decreasing of the crystallite size and percentage value of ZnO crystal indicates a smaller particle size of the GNP/ZnO nanocomposites. Smaller particle size means the surface area of the material is larger, which is related to dipole polarization.

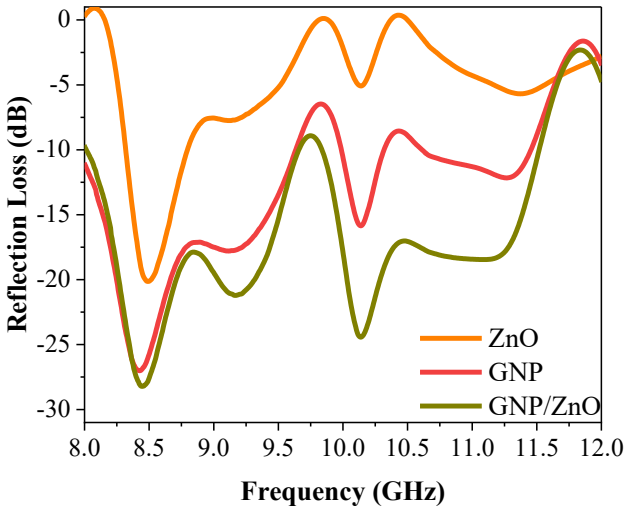

Fig. 7. VNA results of ZnO, GNP, and GNP/ZnO nanocomposites

Based on the microwave absorption performance, the GNP/ZnO nanocomposites were observed as the most suitable material for military radar absorbing material. FE-SEM, XRD, and FTIR results showed that the GNP/ZnO nanocomposites were successfully formed.

Table 3. RL and through power value of the materials

Materials	Frequency (GHz)	Reflection Loss (dB)	Through Power (%)
ZnO	8.48	-20.08	99.08
	9.12	-7.75	83.21
	10.14	-5.08	68.95
	11.37	-5.69	73.02
GNP	8.42	-27.01	99.8
	9.11	-17.79	98.33
	10.13	-15.85	97.4
	1126	-12.16	97.91
GNP/ZnO	8.45	-28.21	99.85
	9.17	-21.21	99.24
	10.13	-24.42	99.63
	11.08	-18.45	98.57

CONCLUSION

The GNP/ZnO nanocomposite was successfully prepared using mechanical homogenization. The disordered crystallite layered structure of the GNP/ZnO nanocomposites was evaluated with FE-SEM and XRD imaging, while the signature functional groups of GNP/ZnO nanocomposites were analyzed with FTIR spectroscopy. These remarkable properties of GNP/ZnO nanocomposites demonstrated their great suitability for military RAMs. The GNP/ZnO nanocomposites exhibited microwave absorption rates of up to 99.8% with the lowest RL of -28.21 dB at 8.45 GHz, when the thickness was 3 mm. Overall, the GNP/ZnO nanocomposites showed outstanding performance as advanced lightweight materials for military RAMs

SUPPORTING INFORMATION

There is no supporting information in this paper. The data supporting this research's findings are available on request from the corresponding author (ABR).

ACKNOWLEDGEMENTS

We acknowledge the support from nanocarbon functional research group, National Innovation, and Research Agency, Tangerang Selatan.

CONFLICT OF INTEREST

There was no conflict of interest in this research.

AUTHOR CONTRIBUTIONS

ABR, AH, GRA, IR, and AS were evenly contributed in this research. This study was designed and performed by ABR, AH and GRA. IR and AS were the manager of characterization. HR and MZP was contributed in revise the manuscript. All authors agreed to the final version of this manuscript.

REFERENCES

[1] Atay, H.Y. & İçin, Ö. 2020. Manufacturing radar-absorbing composite materials by using magnetic Co-doped zinc oxide particles synthesized by Sol-Gel. *J. Compos. Mater.* 54. 4059–4066. doi: 10.1177/0021998320927754.

[2] Wang, X., Zhao, C., Li, C., Liu, Y., Sun, S., Yu, Q., Yu, B., Cai, M. & Zhou, F., 2024. Progress in MXene-based materials for microwave absorption. *J. Mater. Sci. Technol.* 180. 207–225. doi: 10.1016/j.jmst.2023.08.064.

[3] Ruiz-Perez, F., López-Estrada, S.M., Tolentino-Hernández, R.V. & Caballero-Briones, F., 2022. Carbon-based radar absorbing materials: A critical review. *J. Sci.: Adv. Mater. Devices.* 7(3). 100454. doi: 10.1016/j.jsamd.2022.100454.

[4] Elmahaishi, M.F., Azis, R.A.S., Ismail, I. & Muhammad, F.D., 2022. A review on electromagnetic microwave absorption properties: their materials and performance. *J. Mater. Res. Technol.* 20. 2188-2220. doi: 10.1016/j.jmrt.2022.07.140.

[5] Chitraningrum, N., Marlina, R., Arundina, R.Y., Suryani Togatorop, E.R., Sulistyaningsih, S., Arisesa, H., Budiman, I., Daud, P. & Hamzah, M., 2022. Microwave absorption properties of porous activated carbon-based palm oil empty fruit bunch. *AIP Adv.* 12(11). doi: 10.1063/5.0128960.

[6] Panda, S.S.S., Gandi, S., Panigrahi, T. & Parne, S.R., 2023. Investigation of electromagnetic wave absorption properties of Ramphal leaves. *J. Mater. Sci.: Mater. Electron.* 34(15). 1207. doi: 10.1007/s10854-023-10610-8.

[7] Elmahaishi, M.F., Azis, R.A.S., Ismail, I. & Muhammad, F.D., 2022. A review on electromagnetic microwave absorption properties: their materials and performance. *J. Mater. Res. Technol.* 20. 2188-2220. doi: 10.1016/j.jmrt.2022.07.140.

[8] Wang, D.C., Lei, Y., Jiao, W., Liu, Y.F., Mu, C.H. & Jian, X., 2021. A review of helical carbon materials structure, synthesis and applications. *Rare Metals.* 40. 3-19. doi: 10.1007/s12598-020-

01622-y.
[9] Zhang, Y., Heo, Y.J., Son, Y.R., In, I., An, K.H., Kim, B.J. & Park, S.J., 2019. Recent advanced thermal interfacial materials: a review of conducting mechanisms and parameters of carbon materials. *Carbon*. 142. 445-460. doi: 10.1016/j.carbon.2018.10.077.
[10] Gorokhov, G., Bychanok, D., Meisak, D., Shlyk, I., Liubimau, A., Angelova, P., Menseidov, C., Ivanov, E., Kotsilkova, R., Casa, M. & Ciambelli, P., 2019, March. Carbon nanotubes vs graphene nanoplatelets for 3D-printable composites. *IOP Conf. Ser. Mater. Sci. Eng.* 503(1). 012010. doi: 10.1088/1757-899X/503/1/012010.
[11] Yee, K. & Ghayesh, M.H., 2023. A review on the mechanics of graphene nanoplatelets reinforced structures. *Int. J. Eng. Sci.* 186. 103831. doi: 10.1016/j.ijengsci.2023.103831.
[12] Jang, B.Z. & Zhamu, A., 2008. Processing of nanographene platelets (NGPs) and NGP nanocomposites: a review. *J. Mater. Sci.* 43(15). 5092-5101. doi: 10.1007/s10853-008-2755-2.
[13] Cataldi, P., Athanassiou, A. & Bayer, I.S., 2018. Graphene nanoplatelets-based advanced materials and recent progress in sustainable applications. *Appl. Sci.* 8(9). 1438. doi: 10.3390/app8091438.
[14] Liang, Y., Yuan, Y., Wang, B., Wang, Y. & Wei, S., 2021. Microstructure and microwave absorption properties of ZnO with different surfactants by hydrothermal method. *J. Mater. Sci.: Mater. Electron.* 32(21). 25908-25918. doi: 10.1007/s10854-020-05226-1.
[15] Cai, M., Shui, A., Wang, X., He, C., Qian, J. & Du, B., 2020. A facile fabrication and high-performance electromagnetic microwave absorption of ZnO nanoparticles. *J. Alloys Compd.* 842. 155638. doi: 10.1016/j.jallcom.2020.155638.
[16] Paul, N., Jimmy, J., Chakyar, S.P., Simon, S.K., Kizhakooden, J., Bindu, C., Sebastian, A., Umadevi, K.S., Jose, J., Andrews, J. & Joseph, V.P., 2019. Microwave absorption properties of flexible zinc oxide sheet. In AIP Conf. Proc. 2162(1). 020070. doi: 10.1063/1.5130280.
[17] Pohshna, C. & Mailapalli, D.R., 2023. Modeling the particle size of nanomaterials synthesized in a planetary ball mill. *OpenNano.* 14. 100191. doi: 10.1016/j.onano.2023.100191.
[18] Piras, C.C., Fernández-Prieto, S. & De Borggraeve, W.M., 2019. Ball milling: a green technology for the preparation and functionalisation of nanocellulose derivatives. *Nanoscale Adv.* 1(3). 937-947. doi: 10.1039/C8NA00238J.
[19] Chen, Q., Liu, X., Wang, T., Su, X., Liu, M., Chaemchuen, S. & Verpoort, F., 2023. A solvent-free process enabling ZnO/porous carbon with enhanced microwave absorption. *J Mater. Sci. Technol.* 149. 255-264. doi: 10.1016/j.jmst.2022.12.034.
[20] Kholil, M.A., Priyono, P. & Subagio, A., 2022. Multiwalled carbon nanotubes and zinc oxide using a high energy milling method for radar-absorbent. *Mater. Res. Express.* 9(2). 025003. doi: 10.1088/2053-1591/ac4e3a.
[21] Zhang, W., Zheng, Y., Zhang, X., Zhu, Q., Tian, L., Wu, H., Yan, H. & Qi, S., 2019. Structure-microwave absorption performance correlations of GNPs/ZnO nanocomposite absorber: Synthesis, characteration and mechanism investigation. *Ceram. Int.* 45(10). 13376-13384.. doi: 10.1016/j.ceramint.2019.04.033.
[22] Fahri, M., Bolilanga, P.I.W., Gunaryo, G., Stiawan, E. and Kurniadi, T., 2024. Exploring the potential of carbon-based radar absorbing material innovations. *Indones. J. Chem. Stud.* 3(2). 72-81. doi: 10.55749/ijcs.v3i2.56.
[23] Negi, P. & Kumar, A., 2022. Biomass-derived activated carbon/epoxy composite as microwave absorbing material. *J. Electron Mater.* 51(6). 2918-2925. doi: 10.1007/s11664-022-09558-y.
[24] Zheng, H., Zhang, W., Li, B., Zhu, J., Wang, C., Song, G., Wu, G., Yang, X., Huang, Y. & Ma, L., 2022. Recent advances of interphases in carbon fiber-reinforced polymer composites: A review. *Compos. B. Eng.* 233. 109639. doi: 10.1016/j.compositesb.2022.109639.
[25] Setua, D.K., Mordina, B., Srivastava, A.K., Roy, D. & Prasad, N.E., 2020. *Carbon nanofibers-reinforced polymer nanocomposites as efficient microwave absorber*. In Fiber-reinforced nanocomposites: fundamentals and applications. 395-430. Elsevier. doi: 10.1016/B978-0-12-819904-6.00018-9.
[26] Ahmad, I., Nazeri, M.F.M., Salleh, N.A., Kheawhom, S., Erer, A.M., Kurt, A. & Mohamad, A.A., 2021. Selective electrochemical etching of the Sn-3Ag-0.5 Cu/0.07 wt% graphene nanoparticle composite solder. *Arab. J. Chem.* 14(10). 103392. doi: 10.1016/j.arabjc.2021.103392.
[27] Klug, H.P. & Alexander, L.E., 1974. *X-ray diffraction procedures: for polycrystalline and amorphous materials*. ISBN 0-471-49369-4. Wiley-VCH.
[28] Scherrer, P., 1918. Bestimmung der Grosse und inneren Struktur von Kolloidteilchen mittels Rontgenstrahlen. *Nach Ges Wiss Gottingen*. 2. 8-100.
[29] Terinte, N., Ibbett, R. and Schuster, K.C., 2011. Overview on native cellulose and microcrystalline cellulose I structure studied by X-ray diffraction (WAXD): Comparison between measurement techniques. *Lenzinger Berichte*. 89(1). 118-131.
[30] Uzun, İ., 2023. Methods of determining the degree of crystallinity of polymers with X-ray diffraction: a review. *J. Polym. Res.* 30(10). 394. doi: 10.1007/s10965-023-03744-0.
[31] Rajith Kumar, C.R., Betageri, V.S., Nagaraju, G., Pujar, G.H., Onkarappa, H.S. & Latha, M.S., 2020. Synthesis of core/shell (ZnO/Ag) nanoparticles using Calotropis gigantea and their applications in photocatalytic and antibacterial studies. *J. Inorg. Organomet. Polym. Mater.* 30(9). 3410-3417. doi: 10.1007/s10904-020-01507-8.
[32] Jarvin, M., Kumar, S.A., Rosaline, D.R., Foletto, E.L., Dotto, G.L. & Inbanathan, S.S.R., 2022. Remarkable sunlight-driven photocatalytic performance of Ag-doped ZnO nanoparticles prepared by green synthesis for degradation of emerging pollutants in water. *Environ. Sci. Pollut. Res.* 29(38). 57330-57344. doi: 10.1007/s11356-022-19796-6.
[33] Wang, Q., Wang, Y., Meng, Q., Wang, T., Guo, W., Wu, G. & You, L., 2017. Preparation of high antistatic HDPE/polyaniline encapsulated graphene nanoplatelet composites by solution blending. *RSC Adv.* 7(5). 2796-2803. doi: 10.1039/C6RA26458A.
[34] Mahalakshmi, S., Hema, N., Vijaya, P.P. 2020. In vitro biocompatibility and antimicrobial activities of zinc oxide nanoparticles (ZnO NPs) prepared by chemical and green synthetic route—a comparative study. *BioNanoScience*. 10(1). 112-121. doi: 10.1007/s12668-019-00698-w.
[35] Marki microwave. 2016. *Return Loss to VSWR Conversion Table*. 100. 95037.
[36] Sun, X., Wang, Y., Kimura, H., Ni, C., Hou, C., Wang, B., Zhang, Y., Yang, X., Yu, R., Du, W. & Xie, X., 2023. Thermal stability of Ni3ZnC0. 7: As tunable additive for biomass-derived carbon sheet composites with efficient microwave absorption. *J. Colloid Interface Sci.* 642. 447-461. doi: 10.1016/j.jcis.2023.03.194.